

# JWST Near Infrared Spectroscopy of High Albedo Jupiter Trojans: A New Surface Type in the Trojan Belt

MICHAEL E. BROWN,<sup>1</sup> IAN WONG,<sup>2</sup> AND MATTHEW BELYAKOV<sup>1</sup>

<sup>1</sup>*Division of Geological and Planetary Sciences  
California Institute of Technology  
Pasadena, CA 91125, USA*

<sup>2</sup>*Space Telescope Science Institute, 3700 San Martin Drive, Baltimore, MD 21218, MD*

## ABSTRACT

We present 0.8 to 5  $\mu\text{m}$  JWST spectra of four  $\sim 20$  km diameter Jupiter Trojans known to have albedos elevated above the values typical in the remaining Trojan population. The spectra of these four high albedo Jupiter Trojans are all similar, with red slopes in the optical-IR transition region, a break to lower slopes at 1.3  $\mu\text{m}$ , and a broad absorptions from 2.8 to 4  $\mu\text{m}$ . The 0.8 to 2.5  $\mu\text{m}$  spectra of these objects match the spectra of neither the well-known “red” and “less-red” Jupiter Trojans nor of any known asteroid taxonomic class. The reflectivity of these objects does not rise redward of 4  $\mu\text{m}$ , a property that is seen in the previous JWST observations of Jupiter Trojans only in Polymele. Indeed, the high albedo Jupiter Trojan spectra are a good match to that of Polymele, and Polymele is both the smallest Jupiter Trojan in the previous JWST sample and has the highest albedo of the objects in that sample. We conclude that Polymele and the other high albedo Jupiter Trojans represent a third class of Jupiter Trojans not represented in the more heavily-studied larger objects and are perhaps the products of recent disruptions. The Lucy flyby of Polymele in September 2027 will give a direct view of one of this new class of Jupiter Trojans.

## 1. INTRODUCTION

The Jupiter Trojan asteroids are a key population for understanding the dynamical evolution of the early solar system. In the Nice family of dynamical instability models, the Jupiter Trojans are sourced from the same population as the Kuiper belt of the outer solar system and thus should share similar initial compositions (Morbideilli et al. 2005; Morbidelli 2010). The surface compositions of the Kuiper belt objects

(KBOs) and the Jupiter Trojans, however, appear different. KBOs the size of Jupiter Trojans have a wide range of optical colors and have infrared spectra which show evidence of water ice, CO<sub>2</sub>, CO, and organics (Brown et al. 2012; Barucci et al. 2011; Brown & Fraser 2023; De Prá et al. 2024). Jupiter Trojans, in contrast, occupy a narrower range in color (Emery et al. 2011; Wong et al. 2014), and infrared spectra show only a shallow 3  $\mu\text{m}$  absorption, a small signature of organics, and, in one known case, a small CO<sub>2</sub> absorption (Brown 2016; Wong et al. 2024). While these differences are significant, they could all be simple signatures of the dif-

ferences in surface insolation at the locations of the Jupiter Trojans and that of the Kuiper belt. The interior compositions of these objects remain unknown.

One solution to examining interior compositions is to look for collisional fragments. In the Kuiper belt, fragments that are part of the Haumea collisional family have surfaces of nearly pure water ice (Brown et al. 2007), while in the main asteroid belt, even the youngest known collisional family in the main belt, the Karin family, at only  $\sim 6$  Myr old, has family members whose surfaces are indistinguishable from the background population (Harris et al. 2009). At the Jupiter Trojans, the best-studied collisional family – that of (3548) Eurybates – has fragments that are slightly less-red than the rest of the Jupiter Trojan population. Eurybates itself is the only known member of the Jupiter Trojans to show an absorption feature due to  $\text{CO}_2$  (Wong et al. 2024), but the reason for the presence of  $\text{CO}_2$  is unclear, and otherwise family members have no additional identifiable spectral features (De Luise et al. 2010). The Eurybates family, however, appears ancient (Marschall et al. 2022), so  $\sim 1$ -4 Gyr of space weathering could have erased any spectral signatures of the interiors (Thompson et al. 1987; Brunetto et al. 2006).

Spectroscopy of the survivors of more recent collisions could still retain interior spectral signatures. While current collisional models suggest that objects in the  $\sim 1$  km size range should be collisionally active with collisional time scales of under 100 Myr (de Elía & Brunini 2007), a smaller number of larger objects should also have undergone catastrophic collision over the past 100 Myr. Such objects might reveal themselves as having unusual high albedos compared to the rest of the populations.

Simpson et al. (2022) used a combination of thermal emission observations of Jupiter Trojans from the Atacama Large Millimeter Ar-

ray (ALMA) and the Wide-field Infrared Survey Explorer (WISE) to robustly identify a small set of  $\sim 20$  km Jupiter Trojans with albedos significantly elevated over the  $\sim 0.05$  average value of the remainder of the population and suggested that these could be collisional fragments of recent impacts with still-exposed subsurface materials. Here, we obtain 0.8-5.0  $\mu\text{m}$  JWST spectra of four members of this higher-albedo, never previously-observed population and use these spectra to search for signatures of freshly exposed surface materials on these objects.

## 2. OBSERVATIONS

Observations of four higher-albedo Jupiter Trojans were obtained with the Near Infrared Spectrograph (NIRSPEC) on JWST (Jakobsen et al. 2022) using the low-resolution PRISM mode and the integral field unit. This observing mode provides a spectrum from 0.8-5.0  $\mu\text{m}$  with a resolution ranging from 30 to 400. For each target, the JWST-provided ephemeris position was sufficiently accurate that we blindly acquired the targets into the  $3 \times 3$  arcsecond aperture and performed a two-position dither, using a single integration in the NRSIRS2RAPID and other observing conditions are given in Table 1.

After confirming the correct acquisition of the target and the successful execution of the observations, we run the most recent JWST pipeline and calibration files<sup>1</sup> (version 1.14.0; jwst\_01252.pmap) starting with the Step 1 “\_uncal.fits” files. We perform a custom 1/f noise removal on the derived “\_rate.fits” data, as described in (Brown & Fraser 2023), before running the Step 2 pipeline. We extract spectra from the Step 2 “\_s3d.fits” image cube products using a custom point spread function (PSF)-fitting scheme. The PSF of the data is

<sup>1</sup> as of 12 July 2024

**Table 1.** JWST observational parameters

object		date	time	exp	r	$\Delta$	phase	diam	albedo	$\eta$	T <sub>max</sub>
11488	1998RM11	2023-10-24	19:21-19:29	233	5.01	4.32	9.0	22.7	0.09	0.77	191
13331	1998SU52	2024-03-29	18:50-18:57	233	4.70	4.33	11.9	17.7	0.13	0.50	218
42168	2001CT13	2024-04-21	07:12-07:21	350	5.47	5.40	27.7	18.1	0.13	0.78	181
18263	Anchialos	2024-05-10	16:07-16:15	321	5.07	5.03	27.4	20.1	0.10	0.69	195

NOTE—Table parameters include exposure time, in seconds,  $r$ , the heliocentric distance,  $\Delta$ , the distance to JWST,  $r$  (both in AU), diameter (km), the phase (Sun-asteroid-earth angle), in degrees, and albedo, derived from Simpson et al. (2022), and the beaming parameter,  $\eta$ , and maximum temperature,  $T_{\max}$  in degrees K, obtained in this work.

wavelength dependent both because of standard diffraction effects and because of the undersampling of the PSF by the detector pixels coupled with the curvature of the spectrum across the detector. This latter effect causes pixel-level PSF variations at a characteristic wavelength scale of hundreds of pixels in the PRISM mode. To mitigate this and other wavelength-dependent PSF changes, we first perform a wavelength dependent sky subtraction by subtraction the median of the spatial pixels far removed from the target. We next determine the PSF independently at each wavelength by taking a two-dimensional median of the data in a region  $\pm 50$  pixels in the spectral dimension and normalizing the result to an area of unity. The irradiance is then found by fitting the data at each wavelength to the empirically found PSF by using a weighted median – where the weight of each pixel in the median is the amplitude of the PSF at that positions – of the ratio between the two-dimensional data and the PSF. This weighted-median scheme provides a robust method to account for the large number of bad pixels on the NIRSPEC detector at the expense of the  $\sim 25\%$  higher noise associated with the use of a median rather than a mean. The two dither positions are averaged to obtain the final one-dimensional spectra. Observational circum-

stances and properties of the target are shown in Table 1.

The spectra of all targets are shown in Figure 1. In addition, the spectrum of the star SNAP-2, an approximate solar analog (Bohlin et al. 2014), obtained through Program 1128 and reduced identically, is also shown. The majority of the light from the Trojan targets is reflected sunlight, as seen by the similarity between the target spectra and those of the solar analog. Beyond approximately  $4.5 \mu\text{m}$ , thermal emission from the Jupiter Trojans begins to become apparent.

### 3. RESULTS

To examine the reflectance spectra of the targets, we must first remove the contribution from thermal emission. We follow the procedure outlined by Wong et al. (2024). In short, we use the ALMA-derived diameter and geometric albedo of the targets along with the known geocentric and heliocentric distances to create a model of emission based on the Standard Thermal Model (Harris 1998), with the beaming parameter,  $\eta$ , as a free parameter. We model a range of beaming parameters, subtract the derived thermal emission from the observed spectrum, and divide the resultant spectrum by that of the solar analog star to obtain the relative reflectance. We then modify the beaming parameter until a satisfactory fit is obtained. No rigorous pre-

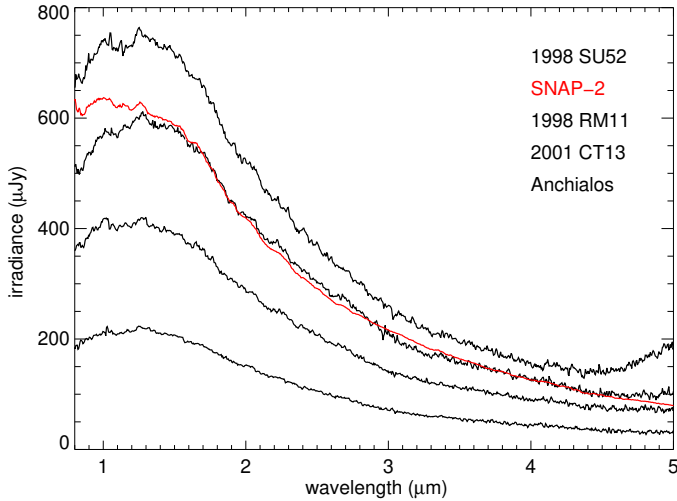


**Figure 1.** Spectra of four high albedo Jupiter Trojans (in black) along with the spectrum of SNAP-2, a solar analog star (in red). The object name associated with each spectrum is shown in the figure in order from brightest to faintest at  $1\ \mu\text{m}$ . The Trojan spectra are dominated by reflected sunlight except for the regions beyond  $\sim 4.5\ \mu\text{m}$ . The relative signal-to-noise across the spectra is determined by the total irradiance and the NIRSpec/PRISM throughput, both of which decrease to longer wavelength. The total uncertainty can be estimated from the scatter in these largely featureless spectra.

description of what makes a fit the most “satisfactory” is possible, as the true reflectance spectrum is not known *a priori*. Based on experimentation with the data, we find that assuming that the reflectance continuum extends from the peak near  $2.7\ \mu\text{m}$  to a line through the spectrum between  $3.8$  and  $5.0\ \mu\text{m}$  and fitting the beaming parameter to minimize positive deviations in this longer wavelength region gives consistent results. Examples of this procedure are shown in Fig 2. This procedure could artificially mask broad spectral features beyond about  $4.2\ \mu\text{m}$ . We keep this caveat in mind when examining the spectra of the objects.

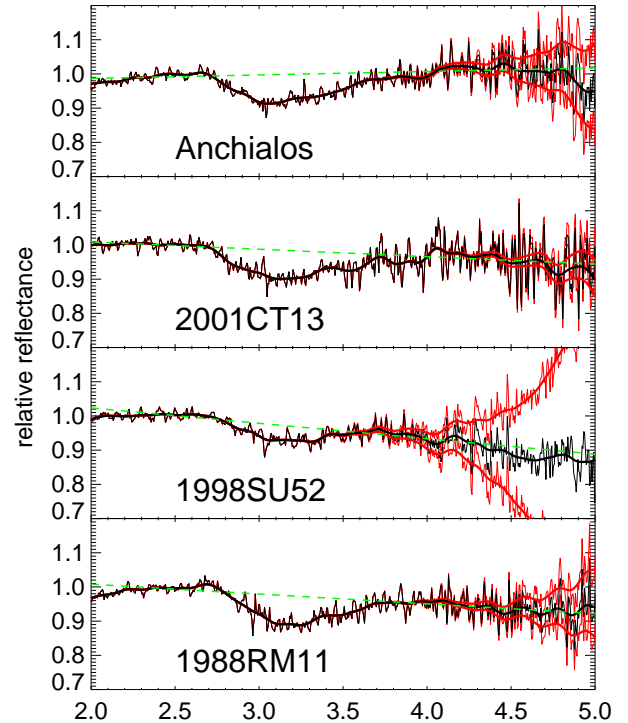


**Figure 2.** Relative reflectivity, scaled to unity between  $2.5$  and  $2.7\ \mu\text{m}$  of the four high albedo asteroids with different choices for the beaming parameter. In each case we show our adopted beaming parameter as a black line and the derived reflectance for a beaming parameter  $0.1$  higher (red curve below adopted reflectance) and one  $0.05$  lower (red curve above adopted reflectance). The green dashed line shows the extension from  $2.7\ \mu\text{m}$  to the region beyond  $3.7\ \mu\text{m}$ , which we use as our estimate of the longer wavelength continuum.

We calculate the absolute reflectivity of these objects by assuming that the linear part of the spectrum from  $0.8$  to  $1.4\ \mu\text{m}$  extends linearly to  $0.55\ \mu\text{m}$  at the center of the  $V$  band where

the albedo is defined. Such a linear slope in this region is characteristic of known Jupiter Trojans and many other small bodies with low albedos (Emery et al. 2011). Absolute reflectivities of the four high albedo Jupiter Trojan targets are shown in Figure 3. Other than slight changes in the absolute level of the reflectivities, the spectra of all 4 targets are similar, with a spectral break at about  $1.3\ \mu\text{m}$ , similar to that on other Jupiter Trojans, and a broad absorption beyond  $2.7\ \mu\text{m}$ , similar to that seen on previous JWST of lower albedo Jupiter Trojans (Wong et al. 2024).

#### 4. DISCUSSION

The spectra of the high albedo Jupiter Trojans do not contain any immediately identifiable absorption features beyond the  $3\ \mu\text{m}$  feature noted by Brown (2016) and Wong et al. (2024). In particular, no hint of water ice, which might be expected to be exposed in a recent impact and which would lead to a heightened albedo, is present. To demonstrate the lack of water ice, in Figure 4, we show a simple model consisting of a linear combination of two spectra. The first component of our model is a spectrum of the large Jupiter Trojan Eurybates (Wong et al. 2024) for which we extend the spectrum linearly below the observed wavelength. This component has an overall albedo of 0.044 (Mottola et al. 2023). The second model component consists of  $10\ \mu\text{m}$  grains of water ice, modeled using optical constants from Clark et al. (2012) and using the technique of Roush (1994), and having an optical albedo of 0.66. Typical water ice grain sizes for dark bodies at this heliocentric distance are even larger (i.e. Stephan et al. 2020), causing deeper absorption features, so our choice of small grains is conservative. To obtain a surface albedo of 0.12, as is typical for these high albedo Trojans, we require a mixture of 85% Eurybates material and 15% of the water ice model. We compare this model spectrum to an average of the four high albedo Trojan spectra, where each spectrum has been scaled to a

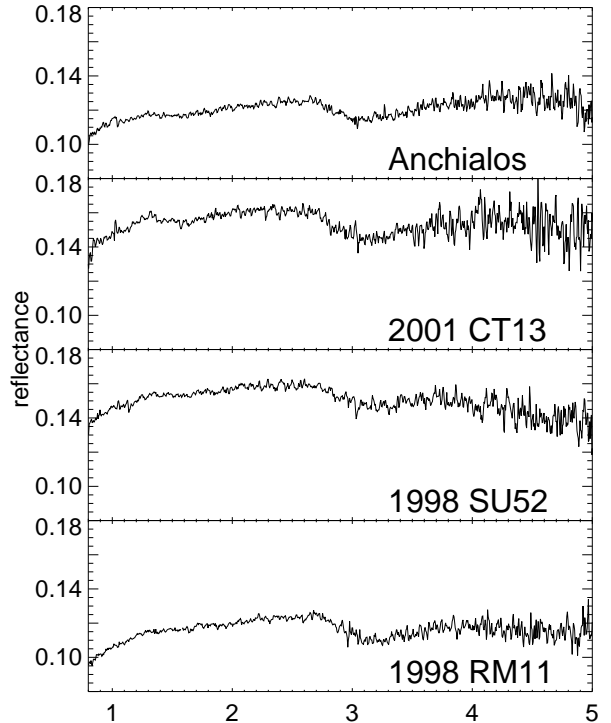


**Figure 3.** Absolute reflectance of four high albedo Jupiter Trojans. The absolute reflectance is determined by assuming that the linear spectrum from  $0.8$  to  $1.3\ \mu\text{m}$  extends downward to  $0.55\ \mu\text{m}$ , where the visible albedo is defined.

value of unity at the median of the values between  $2.5$  and  $2.7\ \mu\text{m}$ , in Figure 4. Such an ice exposure would be readily detected in these spectra. Very little water ice can be exposed on the surfaces of these objects, and exposed water ice cannot account for the heightened albedos.

With no clear spectral signature of newly exposed materials, we turn to comparison with the known spectral properties of other Jupiter Tro-



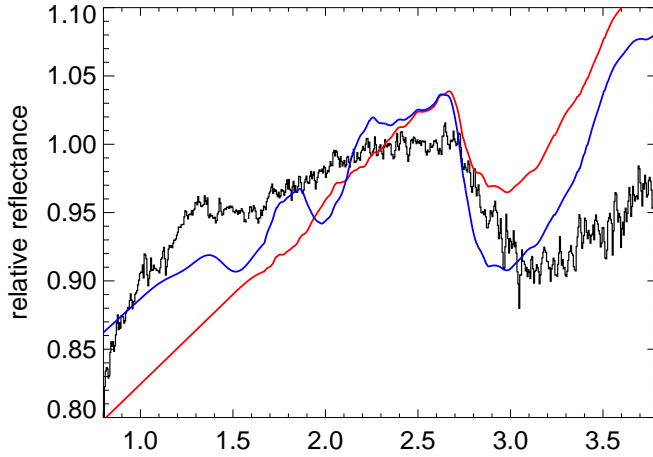


**Figure 4.** The average of the four high albedo Jupiter Trojans, scaled to unity at the median of the value between 2.5 and 2.7  $\mu\text{m}$  (black), compared to a smoothed spectrum of Eurybates (red) and to a model consisting of 85% coverage of Eurybates-like material and 15% water ice (blue), giving an albedo similar to the high albedo Jupiter Trojans.

jans. In Fig. 5 we compare the average high albedo Jupiter Trojan to the average 0.8 to 2.5  $\mu\text{m}$  spectra of the “red” and “less red” classes of Jupiter Trojans from [Emery et al. \(2011\)](#). The high albedo Trojans deviate significantly from either class, with a spectral slope from 0.8 to 1.3  $\mu\text{m}$  similar to that of the red class of Jupiter Trojans, but then a break to a much flatter spectrum than either the red or less-red Trojans out to 2.5  $\mu\text{m}$ . A possible broad absorption from 1.3 to 1.7  $\mu\text{m}$ , unseen in previous Trojan spectra, is also apparent. These feature can be seen, with varying strengths, in all four of the individual spectra. This feature appears among none of the known asteroid taxonomic classes ([DeMeo et al. 2009](#)).

The spectral behaviour of the high albedo Jupiter Trojans beyond 2.5  $\mu\text{m}$  is also unusual. [Brown \(2016\)](#) observed 16 Jupiter Trojans from

2.3 to 3.8  $\mu\text{m}$  using the Keck Observatory, while [Wong et al. \(2024\)](#) observed 5 Trojans from 1.8 to 5.2  $\mu\text{m}$  with JWST. The 3  $\mu\text{m}$  absorption in our high albedo Jupiter Trojan targets has a similar shape and wavelength of those of the other Jupiter Trojans, albeit the absorptions observed here are deeper and extend to longer wavelength than most of those previously seen (Figure 5). These high albedo Trojans lack the 3.4  $\mu\text{m}$  organic feature detected most strongly on (21900) Orus. In addition they have no clear signature of the 4.26  $\mu\text{m}$   $\text{CO}_2$  absorption feature observed exclusively on Eurybates, to date ([Wong et al. 2024](#)).

The largest difference between the high albedo Trojans and the majority of other previously observed Trojans is that in the high albedo Trojans the continuum beyond 2.7  $\mu\text{m}$  is sloped distinctly downward. Among the [Wong et al. \(2024\)](#) JWST sample, only one object – Polymele – is similarly blue-sloped at the longest wavelengths. Indeed, a comparison of Polymele with the average of the high albedo Trojans reveals markedly similar spectral features throughout the range, with the high albedo Jupiter Trojans having an only slightly deeper 3  $\mu\text{m}$  absorption than Polymele.

Interestingly, Polymele is the highest albedo Jupiter Trojan in the [Wong et al. \(2024\)](#) JWST sample and the highest albedo Trojan that will be visited by the Lucy Spacecraft. [Buie et al. \(2018\)](#) give an albedo of 0.074 (compared to an average of  $\sim 0.04$  for the other Lucy targets), but continued occultation results have pushed the surface area even smaller and thus the albedo even higher ([Levison et al. 2023](#)). Polymele is also the smallest of the [Wong et al. \(2024\)](#) sample; at  $\sim 15$  km it is approximately the same size as these high albedo Jupiter Trojans.

In addition to its unusually high albedo, Polymele has an optical color ([Souza-Feliciano et al. 2020](#)) that places it ambiguously between the red and less-red Jupiter Trojan colors ([Wong](#)

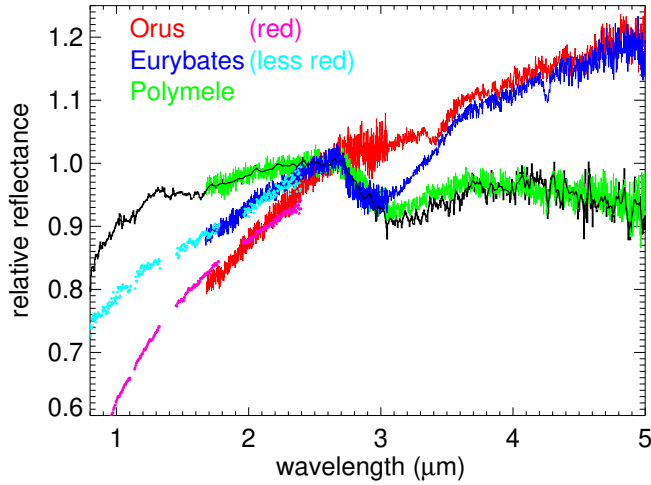


**Figure 5.** Comparison of the average spectrum of the four high albedo Jupiter Trojans (black) to previous Trojan observations. The magenta points show the average of the red Trojan population from Emery et al. (2011) while the cyan points show the average of the less-red population. The JWST spectrum of Orus (red) – a red Jupiter Trojan – shows a weak  $3\ \mu\text{m}$  absorption but a strong  $3.4\ \mu\text{m}$  signature of organics, while Eurybates (blue) – a less-red Trojan – shows a strong  $3\ \mu\text{m}$  absorption and a distinct  $4.26\ \mu\text{m}$  signature of  $\text{CO}_2$  (Wong et al. 2024). The high albedo Jupiter Trojans do not fit into either of these categories. Polymele is the highest albedo object in the Wong et al. (2024) sample and has a spectrum remarkably similar to the other high albedo Jupiter Trojans.

et al. 2014) though it is generally assigned to the class of less-red objects. While the color measurements of the high albedo Jupiter Trojans are not high quality, they are consistent with also being between the two main Jupiter Trojan colors (Schemel & Brown 2021).

The unusual spectral characteristics of these small high albedo Jupiter Trojans and their similarities to Polymele suggests that these are all members of a previously unrecognized class of Jupiter Trojans. This class appears to contain no objects larger than about  $\sim 40\ \text{km}$ , while

most are  $20\ \text{km}$  and smaller. These characteristics remain consistent with the possibility that these are the rare larger objects that have had recent large-scale collisions (Simpson et al. 2022), but no obvious spectral signatures of such collisions are apparent. Wong & Brown (2015) have argued that the collisionally active smallest Jupiter Trojans are consistent in color with the less-red population, inconsistent with the idea that these high albedo objects with mid-red colors are products of collisions. While the true nature of these objects is unclear, the Lucy flyby of Polymele in September 2027 and the comparison with the later flyby targets will give a rare opportunity to help to answer some of the mysteries of these high albedo Jupiter Trojans.

We thank Jessica Sunshine and Rick Binzel for sharing interesting insights into these observations. This work is based on observations made with the NASA/ESA/CSA James Webb Space Telescope. The data were obtained from the Mikulski Archive for Space Telescopes (MAST) at the Space Telescope Science Institute, which is operated by the Association of Universities for Research in Astronomy, Inc., under NASA contract NAS 5-03127 for JWST. These observations are associated with program #2869. Support for program #2869 was provided by NASA through a grant from the Space Telescope Science Institute, which is operated by the Association of Universities for Research in Astronomy, Inc., under NASA contract NAS 5-03127. The specific observations analyzed can be accessed via DOI: 10.17909/j5w3-0d36.

*Facilities:* JWST/NIRSpec.

## REFERENCES

- Barucci, M. A., Alvarez-Candal, A., Merlin, F., et al. 2011, *Icarus*, 214, 297, doi: [10.1016/j.icarus.2011.04.019](https://doi.org/10.1016/j.icarus.2011.04.019)
- Bohlin, R. C., Gordon, K. D., & Tremblay, P.-E. 2014, *Publications of the Astronomical Society of the Pacific*, 126, 711, doi: [10.1086/677655](https://doi.org/10.1086/677655)
- Brown, M. E. 2016, *AJ*, 152, 159, doi: [10.3847/0004-6256/152/6/159](https://doi.org/10.3847/0004-6256/152/6/159)
- Brown, M. E., Barkume, K. M., Ragozzine, D., & Schaller, E. L. 2007, *Nature*, 446, 294, doi: [10.1038/nature05619](https://doi.org/10.1038/nature05619)
- Brown, M. E., & Fraser, W. C. 2023, *PSJ*, 4, 130, doi: [10.3847/PSJ/ace2ba](https://doi.org/10.3847/PSJ/ace2ba)
- Brown, M. E., Schaller, E. L., & Fraser, W. C. 2012, *AJ*, 143, 146, doi: [10.1088/0004-6256/143/6/146](https://doi.org/10.1088/0004-6256/143/6/146)
- Brunetto, R., Barucci, M. A., Dotto, E., & Strazzulla, G. 2006, *ApJ*, 644, 646, doi: [10.1086/503359](https://doi.org/10.1086/503359)
- Buie, M. W., Zangari, A. M., Marchi, S., Levison, H. F., & Mottola, S. 2018, *The Astronomical Journal*, 155, 245, doi: [10.3847/1538-3881/aabd81](https://doi.org/10.3847/1538-3881/aabd81)
- Clark, R. N., Cruikshank, D. P., Jaumann, R., et al. 2012, *Icarus*, 218, 831, doi: [10.1016/j.icarus.2012.01.008](https://doi.org/10.1016/j.icarus.2012.01.008)
- de Elía, G. C., & Brunini, A. 2007, *A&A*, 475, 375, doi: [10.1051/0004-6361:20077979](https://doi.org/10.1051/0004-6361:20077979)
- De Luise, F., Dotto, E., Fornasier, S., et al. 2010, *Icarus*, 209, 586, doi: [10.1016/j.icarus.2010.04.024](https://doi.org/10.1016/j.icarus.2010.04.024)
- De Prá, M. N., Hénault, E., Pinilla-Alonso, N., et al. 2024, *Nature Astronomy*, doi: [10.1038/s41550-024-02276-x](https://doi.org/10.1038/s41550-024-02276-x)
- DeMeo, F. E., Binzel, R. P., Slivan, S. M., & Bus, S. J. 2009, *Icarus*, 202, 160, doi: [10.1016/j.icarus.2009.02.005](https://doi.org/10.1016/j.icarus.2009.02.005)
- Emery, J. P., Burr, D. M., & Cruikshank, D. P. 2011, *AJ*, 141, 25, doi: [10.1088/0004-6256/141/1/25](https://doi.org/10.1088/0004-6256/141/1/25)
- Harris, A. W. 1998, *Icarus*, 131, 291, doi: [10.1006/icar.1997.5865](https://doi.org/10.1006/icar.1997.5865)
- Harris, A. W., Mueller, M., Lisse, C. M., & Cheng, A. F. 2009, *Icarus*, 199, 86, doi: [10.1016/j.icarus.2008.09.004](https://doi.org/10.1016/j.icarus.2008.09.004)
- Jakobsen, P., Ferruit, P., Alves de Oliveira, C., et al. 2022, *A&A*, 661, A80, doi: [10.1051/0004-6361/202142663](https://doi.org/10.1051/0004-6361/202142663)
- Levison, H., Buie, M., Keeney, B., & Mottola, S. 2023, in *AAS/Division for Planetary Sciences Meeting Abstracts*, Vol. 55, *AAS/Division for Planetary Sciences Meeting Abstracts*, 107.05
- Marschall, R., Nesvorný, D., Deienno, R., et al. 2022, *AJ*, 164, 167, doi: [10.3847/1538-3881/ac8d6b](https://doi.org/10.3847/1538-3881/ac8d6b)
- Morbidelli, A. 2010, *Comptes Rendus Physique*, 11, 651, doi: [10.1016/j.crhy.2010.11.001](https://doi.org/10.1016/j.crhy.2010.11.001)
- Morbidelli, A., Levison, H. F., Tsiganis, K., & Gomes, R. 2005, *Nature*, 435, 462, doi: [10.1038/nature03540](https://doi.org/10.1038/nature03540)
- Mottola, S., Hellmich, S., Buie, M. W., et al. 2023, *PSJ*, 4, 18, doi: [10.3847/PSJ/acaf79](https://doi.org/10.3847/PSJ/acaf79)
- Roush, T. L. 1994, *Icarus*, 108, 243, doi: [10.1006/icar.1994.1059](https://doi.org/10.1006/icar.1994.1059)
- Schemel, M., & Brown, M. E. 2021, *PSJ*, 2, 40, doi: [10.3847/PSJ/abc752](https://doi.org/10.3847/PSJ/abc752)
- Simpson, A. M., Brown, M. E., Schemel, M. J., & Butler, B. J. 2022, *AJ*, 164, 23, doi: [10.3847/1538-3881/ac559e](https://doi.org/10.3847/1538-3881/ac559e)
- Souza-Feliciano, A. C., De Prá, M., Pinilla-Alonso, N., et al. 2020, *Icarus*, 338, 113463, doi: [10.1016/j.icarus.2019.113463](https://doi.org/10.1016/j.icarus.2019.113463)
- Stephan, K., Hibbitts, C. A., & Jaumann, R. 2020, *Icarus*, 337, 113440, doi: [10.1016/j.icarus.2019.113440](https://doi.org/10.1016/j.icarus.2019.113440)
- Thompson, W. R., Murray, B. G. J. P. T., Khare, B. N., & Sagan, C. 1987, *J. Geophys. Res.*, 92, 14933, doi: [10.1029/JA092iA13p14933](https://doi.org/10.1029/JA092iA13p14933)
- Wong, I., & Brown, M. E. 2015, *AJ*, 150, 174, doi: [10.1088/0004-6256/150/6/174](https://doi.org/10.1088/0004-6256/150/6/174)
- Wong, I., Brown, M. E., & Emery, J. P. 2014, *AJ*, 148, 112, doi: [10.1088/0004-6256/148/6/112](https://doi.org/10.1088/0004-6256/148/6/112)
- Wong, I., Brown, M. E., Emery, J. P., et al. 2024, *PSJ*, 5, 87, doi: [10.3847/PSJ/ad2fc3](https://doi.org/10.3847/PSJ/ad2fc3)